EVALUATION OF A HYPERSPECTRAL OPTICAL-MONTE CARLO REMOTE SENSING MODEL IN A WATER TANK STUDY

V. Garg, I. Chaubey, S. Singh

ABSTRACT. *A physical hyperspectral optical–Monte Carlo (PHO-MC) model for computing reflectance from a body of water is evaluated in a water tank experiment. Reflectance calculation in the model is simulated based on Monte Carlo simulations of photon packet paths in three dimensions. Simulated reflectance was compared with the measured reflectance. The model was evaluated for varied depths of water and different characteristics of the tank bottom. Significant differences were found in the measured reflectance even for clear water due to change in water depth and bottom reflectance characteristics of the water tank. The model reproduced measured reflectance over the entire spectral region extending from 400 to 800 nm for these varied conditions. Model calculation showed that the effect of diffuse radiation and its specular reflection from the air-water interface contribute significantly to reflectance. The relative error in predicted reflectance for all 41 wavelengths evaluated in this study increased from 5.2% to 25.4% when diffuse radiation and its specular reflections were ignored in the model formulation.*

Keywords. *Hyperspectral model, Monte Carlo simulation, Physical hyperspectral-Monte Carlo model, Remote sensing.*

Optical remote sensing is used for assessing and monitoring the quality of water in lakes, rivers, and other water bodies by making reflectance measurements. In order to extract accurate estimates of water quality parameters, such as suspended matter, chlorophyll concentration, and dissolved organic matter, from measured reflectance, it is critical to have an accurate and reliable remote sensing model based on light-matter interactions. Remote sensing models fall mainly into two categories: empirical and physical. In empirical models, a direct relationship between the measured values of water quality parameters (in terms of their concentrations) and the measured reflectance is developed. Physical models incorporate the actual interactions between light and matter in terms of physical characteristics such as refractive index, scattering, absorption, etc.

A number of empirical models have been reported in the literature to evaluate inland water quality using remote sensing data (Ritchie et al., 1990; Lathrop et al., 1991; Ritchie and Cooper, 1991; Harrington et al., 1992; Schiebe et al., 1992; Choubey, 1994; Ritchie et al., 1994; Yacobi et al., 1995; Fraser, 1998; Allee and Johnson, 1999; Yang et al., 1999; Baruah, 2000; Brivio et al., 2001; Kloiber et al., 2002; Chipman et al., 2004; Panda et al., 2004). However, major drawbacks of these models are variation of model input parameters from one model to other because they are specific to water bodies for which they were developed, and a need for ground-truth data to calibrate and validate the underlying statistical relationships (Marcus and Fonstad, 2007; Sudheer et al., 2006). Moreover, a water quality estimated by an empirical model, such as suspended matter or chlorophyll concentration, has been reported to change over time even for the same location (e.g., Allee and Johnson, 1999). These drawbacks of empirical models are presumably due to the fact that they cannot consider the geometry involved with the observation direction and the solar illumination direction (Morel and Gentili, 1993, 1996), bottom effects (Tolk et al., 2000; Lodhi and Rundquist, 2001; Mobley and Sundman, 2003; Mobley et al., 2003), and vertical variations of the water constituents (Han and Rundquist, 2003; Nanu and Robertson, 2004). In addition, when deriving empirical relationship between one water quality parameter and reflectance, these models ignore the effect of other water quality parameters.

The physical modeling approach is more complex but utilizes the full potential of remote sensing for water quality assessment (Yacobi et al., 1995; IOCCG, 2000; Ritchie et al., 2003). Current interpretations of the complexity of natural bodies of water as optical media are uncertain and controversial (Stramski et al., 2004), suggesting the need for physical models that consider progressively higher degrees of complexity (Morel and Maritorena, 2001). Most of the analytical solutions of physical models are an approximation of the radiative transfer equation described by Mobley (1994). Morel and Prieur (1977) developed a simple

Submitted for review in May 2008 as manuscript number SW 7486; approved for publication by the Soil & Water Division of ASABE in April 2009. Presented at the 2005 ASABE Annual Meeting as Paper No. 052003.

The authors are **Vijay Garg,** Graduate Student, Department of Biological and Agricultural Engineering, University of Arkansas, Fayetteville, Arkansas (currently Chief Scientific Officer, Carbonyx, Inc., Plano, Texas); **Indrajeet Chaubey, ASABE Member,** Associate Professor, Department of Agricultural and Biological Engineering and Department of Earth and Atmospheric Sciences, Purdue University, West Lafayette, Indiana; and **Surendra Singh,** Professor, Department of Physics, University of Arkansas, Fayetteville, Arkansas. **Corresponding author:** Indrajeet Chaubey, Department of Agricultural and Biological Engineering and Department of Earth and Atmospheric Sciences, 225 S. University St., Purdue University, West Lafayette, IN 47907; phone: 765-494-5013; fax: 765-496-1115; e-mail: ichaubey@purdue.edu.

  ISSN 0001–2351

approximate analytical solution of a physical model to calculate reflectance. Similar solutions with some variations in the model form have been considered by others (Gordon et al., 1975; Kirk, 1984; Aas, 1987). These simplified models, generally referred to as semi-empirical models, have found wide applications by researchers (Stramski et al., 2004). However, these models considered radiative transfer of a light beam in one dimension only, used simplified assumption of infinite water depth, and ignored the effect of multiple scattering (Mobley et al., 1993; Mobley, 1994; Stamnes et al., 2003). In addition, validations of these semi-analytical models under standard testing conditions have been lacking.

From the perspective of accuracy, geometric flexibility, and systematic and modular simulation, the most effective approach to solve remote sensing reflectance using a physical model is the Monte Carlo simulation technique (Doyle and Reif, 1998). The differences between analytical approximate solutions and Monte Carlo simulations are the accuracy and computational efficiency of the methods. Even though approximate analytical solutions are computationally efficient, they yield less accurate results. On the other hand, Monte Carlo methods are known to be computationally burdensome due to the large number of simulations involved; however, they have greater accuracy of model output.

Physical models can be used to derive inherent optical properties (IOPs) if concentration data of the optically active constituents (OACs) are collected. This is generally done using inverse modeling in which IOP parameter values are estimated using known concentration or reflectance data. Once the IOP values are known, the model can be applied to estimate reflectance or concentrations using a forward modeling approach. Forward modeling validation of most physical models has relied on a comparison of their performance either with other models or against hypothetical data. It is, however, possible that a remote sensing model can be validated in controlled water tank experiments. To the best of our knowledge, none of the physical models has been used to either verify or explain the dynamics of reflectance in water tank studies under controlled conditions, although many studies have been reported that developed some of the empirical models using water tank experiments (Mantovani and Cabral, 1992; Bhargava and Mariam, 1990; Bhargava and Mariam, 1991a, 1991b; Han and Rundquist, 1996; Han, 1997; Lodhi et al., 1997; Han and Rundquist, 2003). Validation of the remote sensing model with a water tank study can help to identify the accuracy and most significant parameters that need to be considered in the model.

The main objective of this study was to evaluate a physical hyperspectral optical-Monte Carlo (PHO-MC) model by comparing the model-simulated reflectance with the measured reflectance from a water tank study. The measurements were made by changing the water depth to study the effect of water depth, and by changing the bottom characteristics to analyze the effect of bottom conditions. The PHO-MC model was used to study the effect of diffuse light and tank geometry on the prediction accuracy of the model using a forward modeling approach. The model was also used to interpret the light absorption characteristics at different wavelengths and varying water depths.

Materials and Methods

Physical Hyperspectral Optical-Monte Carlo (PHO-MC) Model

A Monte Carlo model code of light propagation in tissue (MCML) by Prahl et al. (1989) was modified to develop the PHO-MC model for this study. In Prahl's MCML model, the photon packet tracing started from the origin (a point at the surface of the tissue) into the tissue by randomly selected trajectory in spherical coordinates. The photon packet was modeled to arrive orthogonally at the tissue surface, and the interaction of the photon packet in the tissue was based on the scattering coefficient of only one OAC in a layer. Inside the tissue, fate of photons was modeled in terms of scattering, absorption, undisturbed propagation, internal reflection, or transmittance out of the tissue. The model recorded the position of the photon when it was absorbed. Similarly, the model recorded the reflection or transmission when the photon escaped from the tissue. The photon could transmit from the bottom of the tissue.

An outline of the PHO-MC model is presented in figure 1. Major modification of the MCML model to develop the PHO-MC model included: (1) starting of photon packet tracing before it hit the water surface, (2) photon packet direction determined based on actual incident light condition, (3) calculation of specular reflection for a photon packet arriving at an angle other than orthogonal angle on the air-water interface, (4) more than one OAC considered in every water layer (fig. 2), and (5) bottom surface modeled as a Lambertian surface. The Monte Carlo method simulates a process under consideration as a stochastic process (Doyle and Rief, 1998). In the PHO-MC model, the process of a photon packet movement and its state were considered as a stochastic process in a three-dimensional space. A photon packet was moved one step, and then its directional and state changes in the medium were defined by suitable probability distributions based on the various optical processes inherent in light-water interaction. Instead of modeling the fate of a single photon, a photon packet is considered in the PHO-MC model to improve the accuracy of Monte Carlo simulations (Mobley, 1994; Prahl et al., 1989). Apparent optical properties (AOP), such as reflectance $R_{rs}(\lambda)$, angular fluxes, radiance, and irradiance, were calculated by averaging the fate of running photon packets a sufficiently large number of times.

Extra inputs were created in the PHO-MC model to provide information about the incident light solar zenith angle, and ratio of diffuse light to total light. Ratio of diffuse light to total light defined the probability of photon packet trajectory as a photon packet of direct light or a photon packet of diffuse light. A random number (ξ, uniformly distributed between 0 and 1) was drawn. If the generated random number was less than the ratio of the diffuse light to the total light, then the photon packet was considered to be from a diffused source; if it was greater, the photon packet was considered to be from a direct source. If the photon packet was from a direct light source, then its direction of incidence on the water surface was the known solar zenith angle. In the case of a diffused light photon packet, its incident direction on the water surface was calculated based on the assumption of uniform distribution of diffused radiance of the downwelling light.

In the PHO-MC model, photon packet interactions with the water surface were included. Once the angle of incidence of the photon packet on the water surface is defined, its final angle of transmission into the water surface was calculated using Snell's law. Also based on incident angle of the photon packet, specular reflection from the water surface was calculated using the Fresnel reflection coefficient. The photon packet weight was reduced from unity by the reflected part before the photon packet entered the water surface. The amount and direction of specular reflection were recorded for the final calculation of reflectance.

In the MCML model, the photon packet was allowed to transmit out from the bottom layer. This was modified in the PHO-MC model. The bottom layer was considered a Lambertian reflecting surface. Therefore, the photon packet hitting the bottom layer was not transmitted out of the water body bottom. Instead, part of it was absorbed and the rest was reflected back. The absorbed part was calculated based on the known optical properties of the bottom layer, which were provided in the model as an extra input.

The MCML model calculated AOP values at one particular wavelength. This was modified in the PHO-MC model to generate a hyperspectral graph of the AOP of an aquatic medium. The MCML model was modified so that the wavelength specific data of IOP values of the aquatic medium can be input for any number of selected wavelengths. The PHO-MC model ran for each set of wavelength-specific data and generated a combined file of AOP output for each wavelength, thus providing hyperspectral data.

Water Tank Experimental Setup

Remote sensing measurements in the water tank were conducted at the Arkansas Agricultural Research and Extension Center (36:05:46.8 N, 94:10:28.5 W NAD83, 1294 ft NAVD88), at the University of Arkansas. The setup

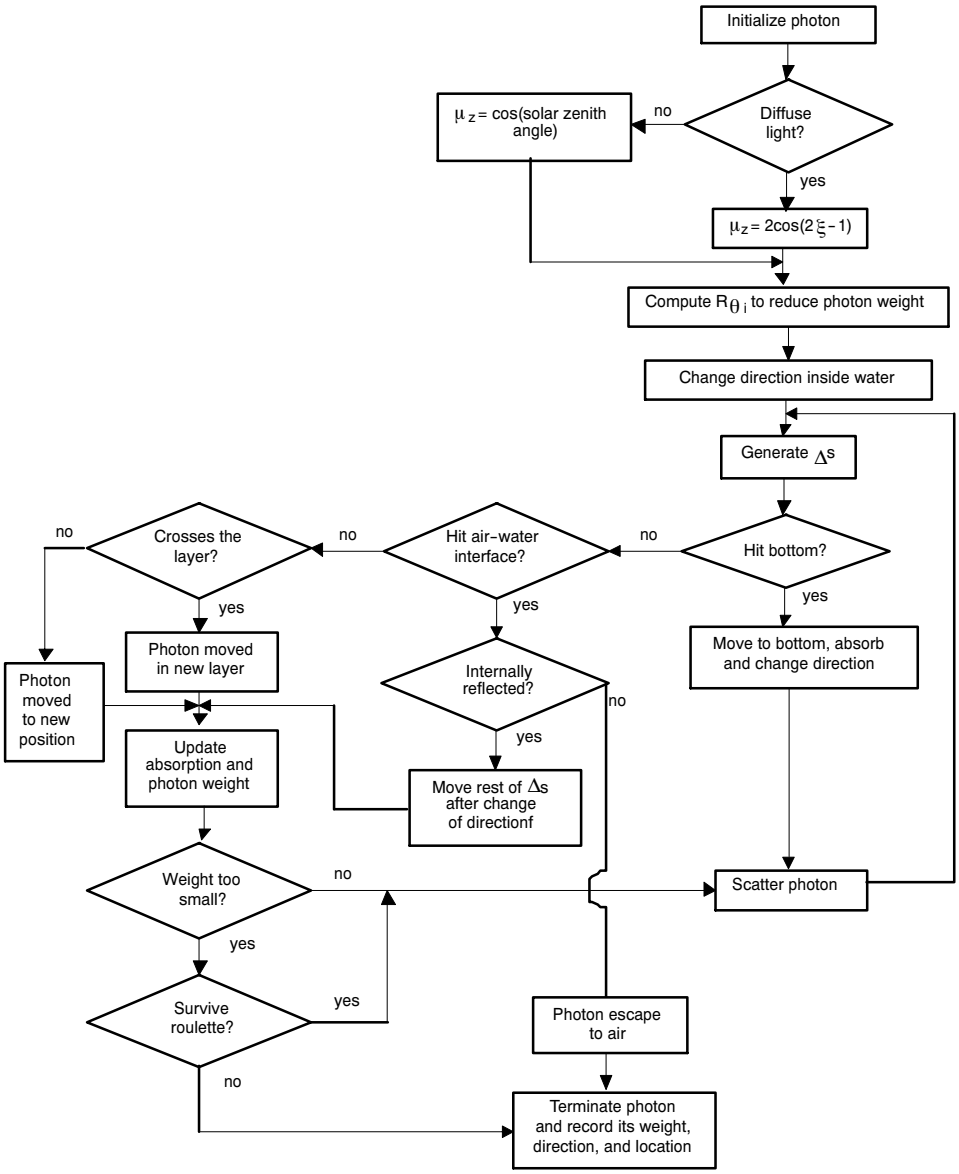

Figure 1. Flowchart of the PHO-MC model for water quality assessment using photon beam random walk in a three-dimensional space. Parameter ξ is a random number uniformly distributed between 0 and 1, Δs is the step size of photon packet movement, and R(θ_i) is the Fresnel reflection coefficient at an angle of incidence θ_i.

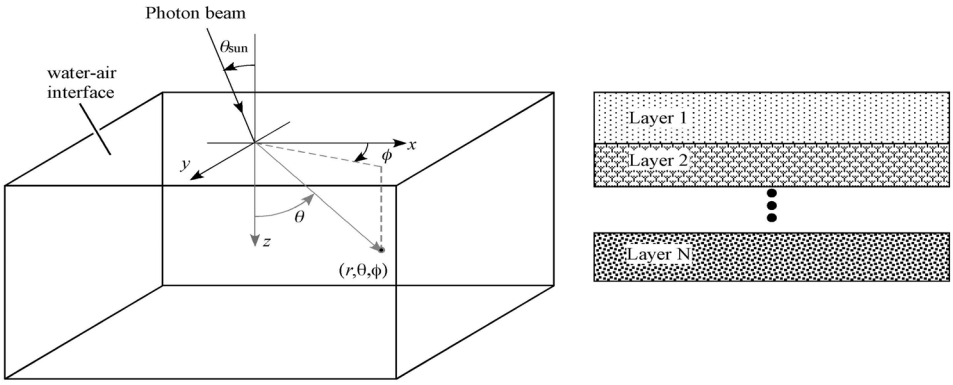

Figure 2. Schematic of the Cartesian (*x*, *y*, *z*) coordinate setup on multilayered water: θ is light angle (θ_{sun} = sun angle or incident direct light angle; θ = angle of transmission), r = unit vector, and φ is azimuth angle.

consisted of a circular tank (1.67 m diameter × 0.80 m height) with the bottom and side walls painted black (fig. 3). The tank was filled with tapwater to depths of 0.10, 0.20, 0.40, 0.50, 0.60, and 0.75 m, and remote sensing measurements were made at each water depth. Afterwards, 1000 g of silty loam soil (USDA: loamy, siliceous, subactive, thermic Lithic Dystrudepts) was added in the tank when the water depth was 0.75 m. The suspended matter was allowed to settle to the bottom of the tank. On the next day, reflectance measurements were taken when the water in the tank was clear and the sediment had settled to the tank bottom.

The reflectance measurements were made using a dual-sensor spectroradiometer (ASD FieldSpec Pro, Analytical Spectral Devices, Inc., Boulder, Colo.). All measurements were made outdoors under natural light conditions. Data were collected in the wavelength range of 400 to 800 nm at 1.438 nm intervals using two sensors, i.e., reference sensor and target sensor, simultaneously. The reference sensor is used for calibration reference, and the target sensor is used for reflectance measurement of a target. The reference sensor of the instrument measured downwelling solar radiance, $L_u(\lambda)$, at wavelength λ from a Lambertian Spectralon reference panel. The reference sensor had a 25° field of view. It was mounted 0.03 m above the Spectralon reference panel, resulting in a circular view of 0.013 m diameter. The target sensor, with an 8° field of view, measured upwelling radiance, $L_w(\lambda)$, of the target surface. The target sensor was placed 0.3 m above the water surface and positioned in the nadir direction for the 0.75 m water depth. The position of the target sensor was kept constant; therefore, the distance between the target sensor and the water surface varied for data collected at other water depths. No artificial lighting was provided in the setup; only the natural light was used. Data were collected on 17-18 October 2003 under clear sky conditions during 1100 h to 1200 h. From the measured values of $L_u(\lambda)$ and $L_w(\lambda)$, the reflectance, $R(\lambda)$, was calculated as:

$$R(\lambda) = 100 \cdot \frac{L_w(\lambda)}{L_u(\lambda)} \quad (1)$$

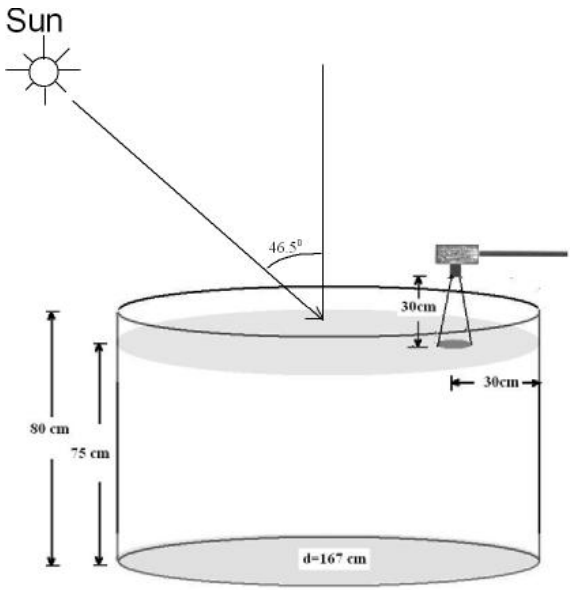

Figure 3. Outline of the experimental setup for water tank study.

The reference sensor measured the total light. To measure the diffuse light, $L_d(\lambda)$, we blocked the direct light by placing a black opaque sheet between the sun and the reference panel using the method given by Singh et al. (2008). The diffused light ratio was calculated as $L_d(\lambda)/L_u(\lambda)$.

The reflectance of the black surface at the tank bottom was measured before filling the tank in order to provide measured bottom characteristics as input in the PHO-MC model. The measured bottom reflectance is shown in figure 4a. Dry silty loam soil used in the experiment was spread in a 0.01 m thick layer over a black surface, and its reflectance, $R_{Soil}(\lambda)$, was measured (fig. 4b). The ratio of diffused light to total light, $r_D(\lambda)$, was computed by the measurements done by the reference sensor (fig. 5). It was clear that the black surface at the bottom had almost constant reflectance (2%) over all wavelengths between 400 and 800 nm. Sun zenith angle was obtained for the date, time, and location of the experiment from the Astronomical Applications Department of the U.S. Naval Observatory (http://aa.usno.navy.mil/; assessed on 30 Aug. 2006). The average value of the sun's zenith angle was 46.5° during the experiments. The refractive index of air was 1.000. The refractive index of water at different wavelengths was taken from Mobley (1994) and varied from 1.344 to 1.331, over the 400 to 700 nm wavelength range at 10°C for fresh water. For wavelengths beyond 700 nm, the water refractive index was assumed equal to its value at 700 nm.

The values of pure water scattering coefficient $b_w(\lambda)$ were taken from Smith and Baker (1981), which are commonly employed for remote sensing studies (Stramski et al., 2004).

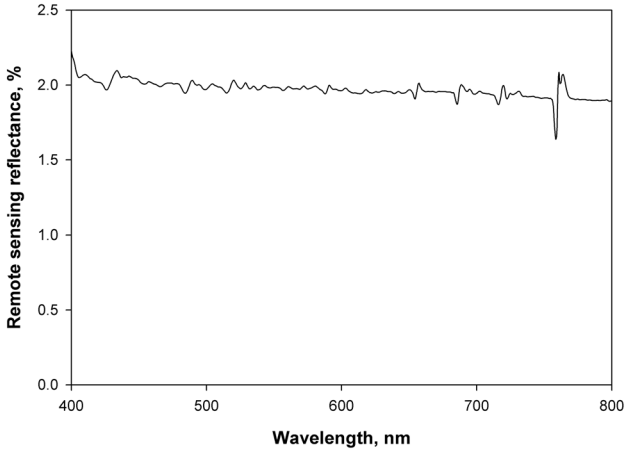

Figure 4a. Reflectance of the black painted bottom of the water tank.

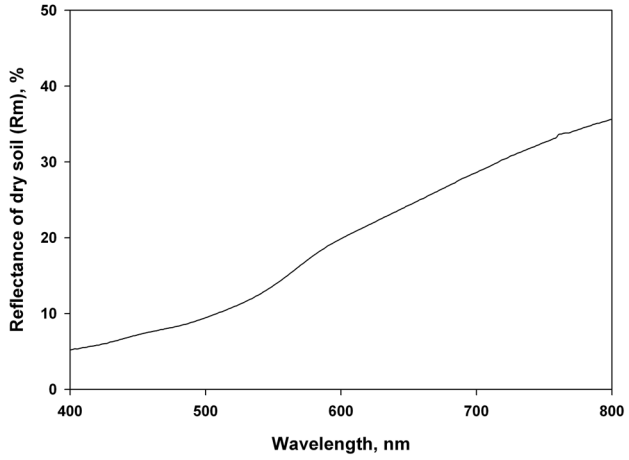

Figure 4b. Reflectance, $R_{soil}(\lambda)$, of 0.01 m thick layer of dry soil spread over a black surface.

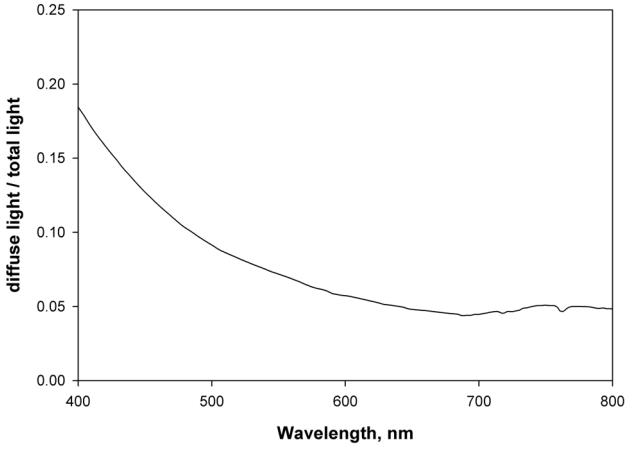

Figure 5. Ratio of diffuse light to total light at the time of water tank study at 11:30 a.m. on 17 October 2003.

The values of absorption coefficient $a_w(\lambda)$ over the wavelength range 400 to 700 nm were obtained from Pope and Fry (1997). It should be noted that Pope and Fry (1997) did not have the $a_w(\lambda)$ values for the 700 to 800 nm wavelength range; these values were taken from Smith and Baker (1981).

To reduce the level of statistical noise, the PHO-MC model was run for many unit-weight photon packets. To ascertain the level of statistical noise, the PHO-MC model was run five times for the same model inputs and number of photon packets. The PHO-MC model results varied each time, as expected from a stochastic model. This variation of the PHO-MC model reduced as the number of photon packets used increased. Table 1 presents the reflectance and its statistical uncertainty when 10^5, 10^6, and 10^7 photon packets were used to simulate the reflectance ($R_S(570)_{0.75}$, i.e., simulated reflectance at 570 nm wavelength and 0.75 m water depth) five different time for each set of photon packet numbers. The standard deviation of $R_S(570)_{0.75}$ decreased as the number of photon packets increased for the simulation. The variance of $R_S(570)_{0.75}$ for 10^7 photons was 0.62. The computational time required for the model to complete tracing of a single photon packet trajectory was typically 4 μs. This was low enough for carrying out large sample calculations. The total number of photon packets used in the PHO-MC model based on these results was 10^7, as this allowed to complete hyperspectral reflectance simulation at 41 wavelength in about 27 min of computer time.

Table 1. Dependence of statistical noise in the PHO-MC predicted reflectance on the number of photon packets used for simulation. The PHO-MC model was run five times for each number of photon packets keeping all the input parameters constant.

No. of Photon Packets in Simulation	Mean Reflectance (M, %)	Standard Deviation (SD)	Coefficient of Variance (CV) (= M × 100/SD)
10^5	2.05	0.28	13.72
10^6	1.95	0.08	3.97
10^7	1.89	0.01	0.62

Results and Discussion

Effect of Water Depth

The PHO-MC model was run to simulate reflectance $R_S(\lambda i)_{dj}$ at six different water depths (dj = d1 to d6) and 41 different wavelengths (λi = λ1 to λ41). The six water depths were 0.75, 0.60, 0.50, 0.40, 0.20, and 0.10 m, and the 41 wavelengths ranged from 400 to 800 nm at 10 nm intervals. The original reflectance data collected at 1.438 nm intervals was used to resample data at the wavelengths of the study using resampling software provided with the spectro-radiometer. Measured reflectance of the black tank bottom and measured total light and diffuse light levels at the time of the experiment were used as inputs in the model. Geometric corrections due to the finite horizontal extent of each water layer were applied by including only the photon packets emerging from a circular area within the area of the tank. Figure 6 presents the measured $R_M(\lambda i)_{dj}$ versus PHO-MC model simulated reflectance, $R_S(\lambda i)_{dj}$, of the water surface for 246 conditions (due to the six water depths and 41 wavelengths) of the study. The overall simulation error (RE, %) was computed as the average of the relative error of simulation across the entire range of wavelengths and depths as:

$$RE = 100 \sum_{i=1}^{i=41} \sum_{j=1}^{j=6} \frac{\left| R_M(\lambda i)_{dj} - R_S(\lambda i)_{dj} \right|}{R_M(\lambda i)_{dj}} \qquad (2)$$

A rather low value of RE (6%), a significant Pearson product-moment correlation coefficient ($r = 0.99$, $p < 0.01$),

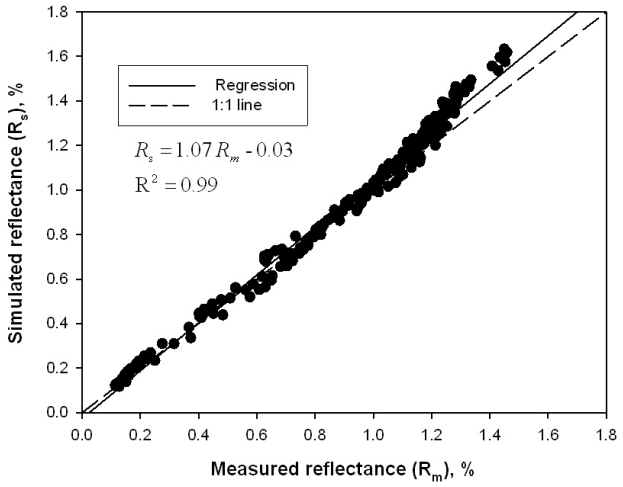

Figure 6. PHO-MC model simulated reflectance ($R_S(\lambda i)_{dj}$) versus measured reflectance ($R_M(\lambda i)_{dj}$) of the clear water surface in a tank study for 246 combinations of six different water depths (d*j* = d1 to d6) and 41 different wavelengths (λi = λ1 to λ41). The six water depths were 0.75, 0.60, 0.50, 0.40, 0.20, and 0.10 m, and the 41 wavelengths ranged from 400 to 800 nm at 10 nm intervals.

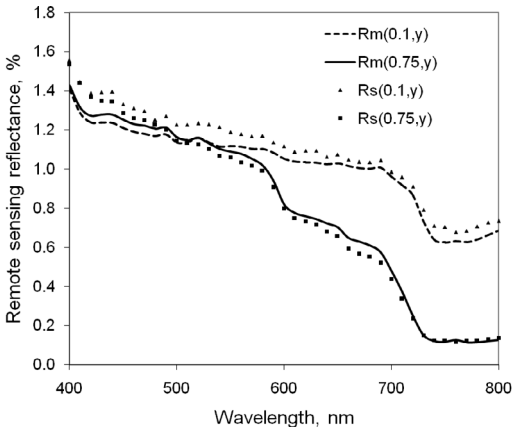

Figure 7. Measured and PHO-MC model simulated reflectance for 0.75 and 0.1 m water depths in a tank with a black bottom. $R_M(\lambda)_{0.1}$ represents measured reflectance at 0.1 m water depth and wavelength (λ). $R_S(\lambda)_{0.1}$ represents PHO-MC model simulated reflectance at 0.1 m water depth and wavelength (λ).

a near-one value of the regression coefficient (1.07), and a small offset (-0.03) of the regression line illustrate the effectiveness of the remote sensing model for simulating reflectance at any of the wavelengths in the rage of 400 to 800 nm of the visible light spectrum and at varying depths of water. The RE of 6% may be due to the assumption of uniform radiance of downwelling diffused light on the water surface, the Lambertian surface assumption for the bottom of the tank, the use of tapwater that was modeled as pure water, and/or instrumental error.

Reflectance values in general decreased at all wavelengths when the water depth increased. Figure 7 presents the reflectance for the maximum and minimum water depths of the study. Decrease in reflectance values for deeper water was greater in the red and infrared wavelength regions. This higher reduction is due to a sharp increase in the water absorption characteristics in the red and infrared regions. Therefore, water depth can be a significant factor affecting the reflectance in a shallow water body, and this model can account for these changes in reflectance due to water depth. The model should also be able to accurately capture the reflectance behavior of deeper water bodies since it is a physics-based model and has capabilities to account for bottom characteristics (described below) and horizontal and vertical dimensions of the water body. The results of the model validations with known optical properties of materials present in a deep water body (Beaver Reservoir) located in Arkansas are provided by Garg (2006) and Garg et al. (2009).

Effect of Bottom Characteristics

Measured remote reflectance of 0.75 m deep clear water with a black painted tank bottom, $R_M(\lambda)_{0.75(\text{black bottom})}$, was significantly different (fig. 8) from measured reflectance of similar 0.75 m deep clear water with the tank bottom covered with suspended sediments, $R_M(\lambda)_{0.75(\text{sed bottom})}$. The value of $R_M(\lambda)_{0.75(\text{sed bottom})}$ was higher at all wavelengths compared to $R_M(\lambda)_{0.75(\text{black bottom})}$. This variation in reflectance due to different bottom characteristics of a shallow clear water body shows the importance of considering bottom characteristics in remote sensing models. These results indicate that change in the reflectance characteristics of a water body bottom can significantly change the reflectance of that water body, especially if the water body is shallow and has comparatively clear water.

The PHO-MC model was used to simulate the reflectance of 0.75 m deep water for the case when the tank bottom was covered with sediments, $R_S(\lambda)_{0.75(\text{sed bottom})}$. For this simulation, reflection characteristics of the black bottom (fig. 4a) were replaced in the input parameter values of the PHO-MC model with the measured reflection characteristics of dry soil (fig. 4b). Simulated and measured reflectance values from the 400 to 800 nm wavelength range at 10 nm intervals were compared. Figure 9 presents the measured $R_M(\lambda)_{0.75(\text{sed bottom})}$ versus PHO-MC model simulated reflectance, $R_S(\lambda)_{0.75(\text{sed bottom})}$, of the water surface for the 41 wavelengths of the study. A significant Pearson product-moment correlation coefficient ($r = 0.97$, $p < 0.01$), a near-one value of regression coefficient (0.92), and a small offset (0.58) of the regression line between $R_S(\lambda)_{0.75(\text{sed bottom})}$ and $R_M(\lambda)_{0.75(\text{sed bottom})}$ illustrate the effectiveness of the remote

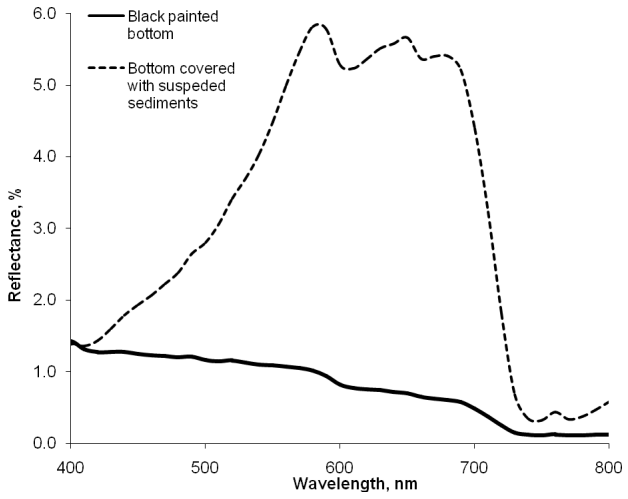

Figure 8. Measured reflectance at 0.75 m clear water depth in a water tank study with a black painted tank bottom and with the tank bottom covered with suspended sediments.

sensing model for simulating the reflectance when bottom reflection characteristics were changed. This shows the model's flexibility in accounting for variations in water body bottom characteristics, which may be an important consideration in a shallow water body.

Effect of Diffuse Light and Tank Geometry

The hyperspectral spectrum of reflectance of water surface simulation in the PHO-MC model considers the diffused light, the specular reflection of diffused light, and the actual boundary conditions of the tank studies (set 1). This section identifies the error introduced in the reflection simulation by ignoring all or some of these. For this discussion, the 0.75 m water depth in the experimental tank is considered. The simulated reflectance for this case (set 1) as a function of wavelength, $R_S(\lambda)_{0.75(set\,1)}$, is compared with the measured reflectance, $R_M(\lambda)_{0.75}$, in figure 10a. The reflectance predicted by the PHO-MC model reproduced the measured values quite well at all wavelengths. The overall simulation relative error, $RE_{0.75(set\,1)}$, of simulation across the entire range of 41 wavelengths is low (5.2%).

The flexibility of the model allowed investigating the effect of other variables. For example, when diffused light was ignored in the PHO-MC model simulations and no adjustments were made due to sensor location (set 2), the $RE_{0.75(set\,2)}$ was found to be 25.1%. This is considerably higher compared to set 1. The simulated reflectance for this case, $R_S(\lambda)_{0.75(set\,2)}$, is compared with the measured reflectance, $R_M(\lambda)_{0.75}$, in figure 10b. It is clear from this figure that the simulated results deviate from measured values at all wavelengths. The assumption used in set 2 of all downwelling light being direct light is common in many modeling exercises due to the absence of measured information on diffused light. It is also worth noting that the model underestimates the reflectance at all wavelengths. A significant error in the modeled reflectance when the diffuse light is ignored indicates that the reflectance cannot be accurately modeled using only direct light (fig. 10b).

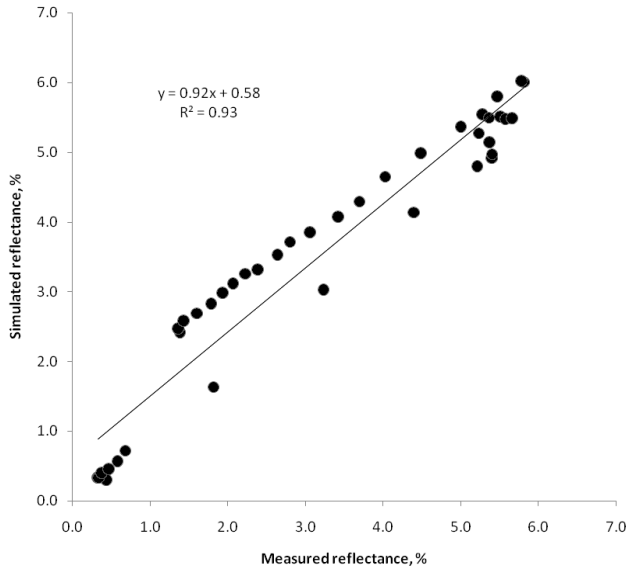

Figure 9. PHO-MC model simulated reflectance $R_S(\lambda)_{0.75(sed\ bottom)}$ versus measured reflectance $R_M(\lambda)_{0.75(sed\ bottom)}$ of the clear water surface in a water tank study for a water depth of 0.75 m and with the tank bottom covered with soil. Hyperspectral reflectance was simulated at 41 different wavelengths (λ) ranging from 400 nm to 800 nm at 10 nm intervals.

Another model simulation was run (set 3) in which measured diffused light was included in the model input parameters but specular reflection of the diffuse light was not considered in calculating the reflectance. The simulated reflectance, $R_S(\lambda)_{0.75(set\,3)}$, for set 3 is presented in figure 10c, along with the measured reflectance, $R_M(\lambda)_{0.75}$. It is observed that the RE of set 3 increased slightly, from 25.1% for set 2 to 25.4% for set 3.

In set 4, the values of diffused light specular reflection were added to the reflectance of set 3. The simulated reflectance, $R_S(\lambda)_{0.75(set\,4)}$, for set 4 followed the measured $R_M(\lambda)_{0.75}$, as presented in figure 10d. The contribution of diffused light to specular reflection for the current study was computed by using the Fresnel equation and the measured ratio of diffused to direct light for the nadir-viewing 8° foreoptic target sensor. It is to be noted that the simulated reflectances of sets 2 and 3 were always lower than the measured reflectance (figs. 10b and 10c). Adding diffused light specular reflection explained some of the missing reflectance component of sets 2 and 3. This indicates that, if specular reflection of diffused light is ignored, model simulations will underestimate the reflectance. After adding diffused light specular reflection, the relative error, $RE_{0.75(set\,4)}$, decreased further to 7.2%, a significant improvement over the value 25.4% for set 3. This shows the importance of including the contribution of diffused light specular reflection to reflectance. These results show that when diffused light is present, its specular reflected component needs to be accounted for in the model. Doxaran et al. (2004) also reported that surface reflection effect is predominant, and approximate correction leads to large errors in the retrieved water-leaving signal.

Note that when diffused light specular reflection was incorporated in the model (set 4), the simulated values were on the higher side compared to the measured values at all wavelengths (fig. 10d). This is in contrast to set 3. Another important observation from figure 10d is that the simulated values deviate most from the measured values in the wavelength range 400 to 570 nm. In fact, this region contributes most to the overall RE of 7.2%. Lower wavelengths near 400 nm contribute more to the RE, and the contribution decreases as the wavelength increases. In the wavelength range 400 to 570 nm, the water absorption coefficient is very low, while the scattering coefficient has a high value. This implies that photons can travel long distances before they are terminated. Due to this long free path, the photon packet may emerge from the water at a point far from the entry point. Since the tank experiment has a finite extent, and the side walls are black, the far-traveling photons are absorbed and do not contribute to upwelling radiance. This suggests that the assumption of infinite extent of layers in the current model needs to be modified to account for the boundary conditions in the experiment. When we accounted for the actual boundary conditions of the tank, the RE decreased to 5.2%. These results indicate the importance of accounting for shoreline boundary conditions in modeling the reflectance of a body of water.

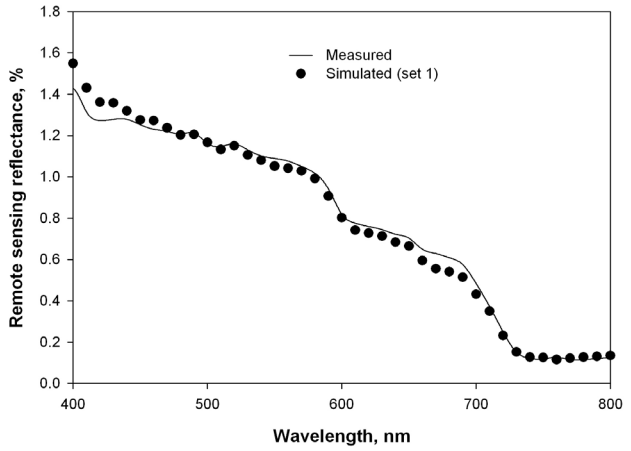

Figure 10a. Measured and PHO-MC model simulated reflectance (set 1) for 0.75 m water depth. In set 1, light consisted of direct as well as diffused components. Diffused light specular reflection from the air-water interface was added to the simulated reflectance. Water tank side wall correction was also incorporated in the PHO-MC model.

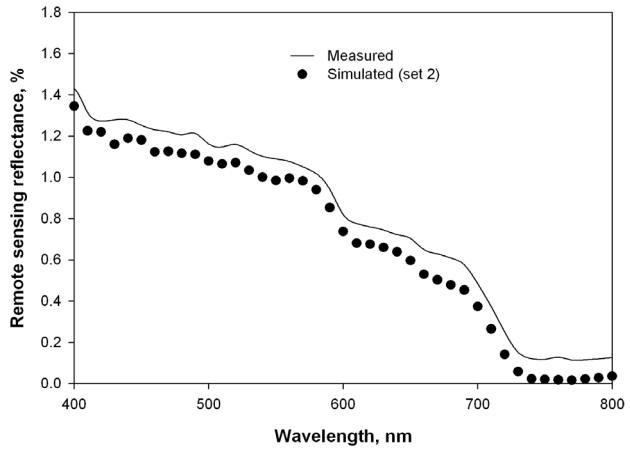

Figure 10b. Measured and PHO-MC model simulated reflectance using only direct light (set 2) for 0.75 m water depth. In set 2, diffused light and boundary conditions of the experimental tank were ignored to compare the model accuracy with the set 1 condition (fig. 10a).

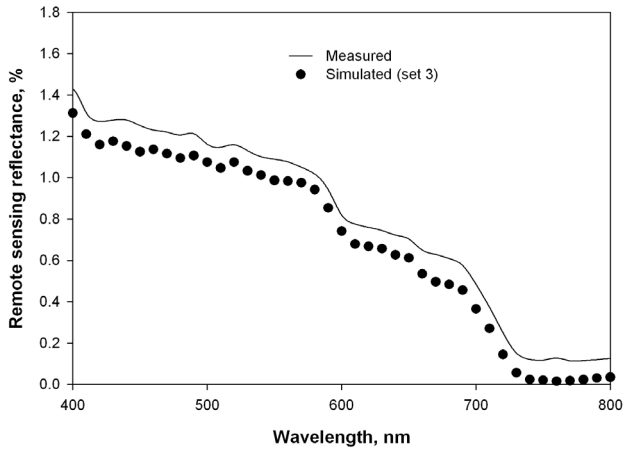

Figure 10c. Measured and PHO-MC model simulated reflectance including direct as well as diffused light (set 3) but without specular reflection for 0.75 m water depth. In set 3, specular reflection of diffused light and the boundary conditions of the experimental tank were ignored to compare the model accuracy with sets 1 and 2 conditions (figs. 10a and 10b).

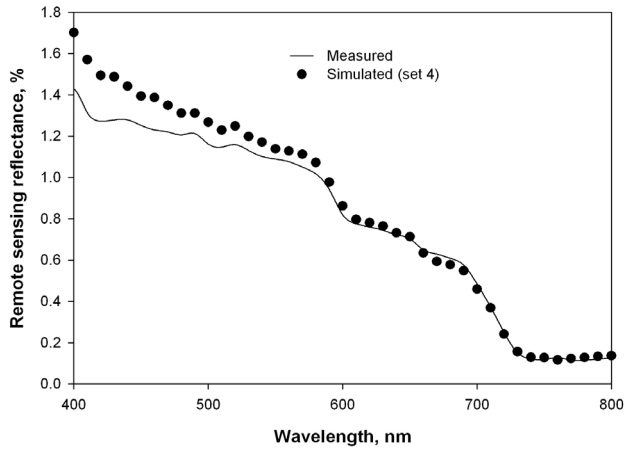

Figure 10d. Measured and PHO-MC model simulated reflectance with direct and diffused light when specular reflection of diffused light is included in the PHO-MC model (set 4) for 0.75 m water depth. In set 4, boundary conditions of the experimental tank were ignored to compare the model accuracy with sets 1, 2, and 3 conditions (figs. 10a, 10b, and 10c).

Interpretation of Energy Absorption along Water Depth

The PHO-MC model was used to calculate the absorption pattern of different wavelengths of light along the water depth and at the tank bottom. The model was also used to identify the percent contribution to the reflectance by light at different radial distances from the measurement point.

Figure 11 shows the percent cumulative absorption of light for the 400 to 800 nm wavelength range from the surface to the 0.75 m water depth. The rest of the light was absorbed by the black bottom of the tank. Due to the lower absorption coefficient of water for 400 to 450 nm wavelength light, most of the absorption occurred at the bottom of the tank. However, most of the infrared light was absorbed along the depth.

It is interesting to note that the light entering at approximately 0.80 to 0.90 m distance from the point of observation contributed more to the reflectance than the light entering near the point of observation (fig. 12). The light about 0.70 to 0.80 m away from the point of observation is the probably the light that reaches the bottom and then reflects up, contributing to the reflectance. This may be an important consideration whenever reflectance data are collected in a water body using an observation platform such as a boat. The observation platform on which the target sensor is mounted should not be within -90° to 90° azimuth angle and should not block the light that may actually be contributing more of the reflectance at the measurement point. This information is also important for showing that the reflectance near the sides of the water body will have a different reflectance spectrum due to absence of light from one side of the water body.

Application of PHO-MC Model for Water Quality Assessment

Rapid assessment of water quality and hydrologic conditions over greater temporal and spatial scales is one of the main advantages of remote sensing models compared to traditional *in situ* data collection and laboratory analyses. Accurate interpretation of remote sensing signals to derive water quality information requires knowledge of the inherent optical parameters (IOPs) of water and its optically active

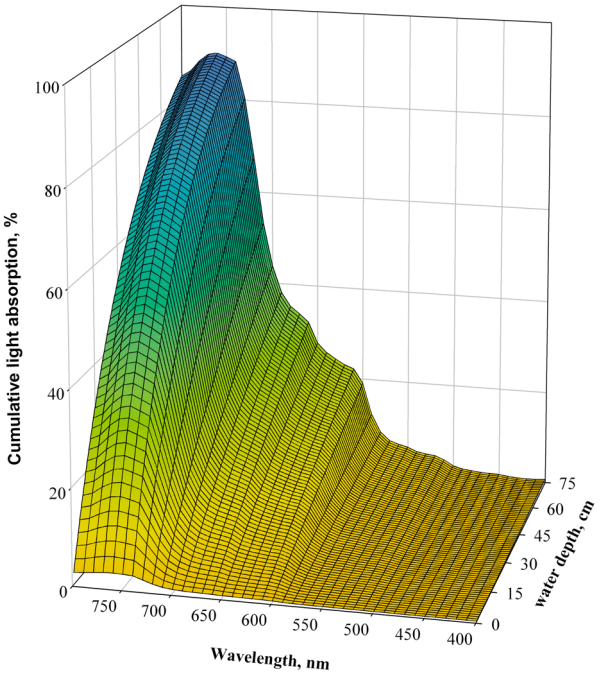

Figure 11. PHO-MC model predicted distribution of percent cumulative light absorption from the surface to 0.75 m below the surface in a water tank study. The rest of the light was absorbed by the black bottom of the tank.

constituents (OACs). The PHO-MC model can be used to determine the IOP of OACs by inverse modeling. Generally, assessment of suspended matter IOP values is one of the most difficult problems to solve (Arst, 2003), primarily because suspended matter is a mixture of organic (dead algae, humic particles, detritus, bacteria, virus) and mineral particles. Further, there exists a great variability in the constituents of suspended matter from one water body to another, and temporal variability within the same water body.

If the OAC concentration data are collected, then the PHO-MC model can be effectively utilized to determine IOPs using an inverse modeling approach. Garg et al. (2009) successfully determined the IOP of suspended matter for concentrations ranging from 0.24 to 560 g m^{-3} using the PHO-MC model with an inverse modeling approach. Once the IOPs of the OACs in the water are known, the PHO-MC model can be used to estimate concentrations of OACs based on measured reflectance data and known IOPs either by using forward modeling or by generating a library of spectral look-up tables that relate observed spectral reflectance to the characteristics of the water column, such as bottom type, water depth, and concentrations of DOM, suspended matter, and chlorophyll. A successful application of the PHO-MC model in estimating the concentrations of SM, DOM, and chlorophyll in the Beaver Reservoir in Arkansas is provided by Garg (2006) and Garg et al. (2009). Many other researchers have successfully demonstrated estimation of water quality parameters and their IOPs using these approaches and Hydrolight, a commercially available remote sensing model (Mobley et al., 2005; Marcus and Fonstad, 2007).

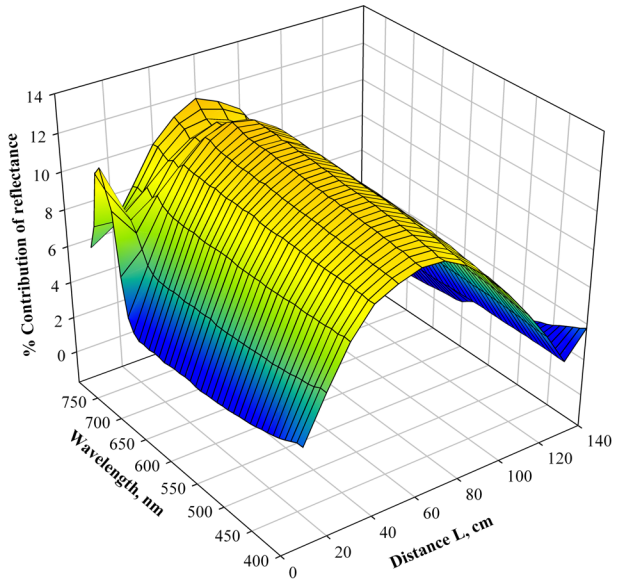

Figure 12. PHO-MC model predicted contribution to reflectance of a point at a distance L from the point of observation.

Summary and Conclusions

A physical PHO-MC model based on three-dimensional simulations of photon paths was used to calculate reflectance in a water tank study. The model was capable of calculating reflectance from a multilayered body of water. The model was flexible to adopt for variation of solar zenith angle, water depth, bottom characteristics of the water body, and diffused light in addition to direct light. To reduce statistical errors and improve simulation time, the PHO-MC model used a photon packet instead of a single photon, and a variable step size instead of a fixed step size for photon packet movements. The statistical noise (coefficient of variance) and time of run were 0.6 and 4 μs, respectively. The model was tested and validated by conducting reflectance measurements on a tank of water at the University of Arkansas. The model reproduced experimentally measured reflectance over the spectral range of 400 to 800 nm and tank water depths of 0.10 to 0.75 m with overall relative errors of 6%. Significant correlation was found between the model-simulated reflectance and measured reflectance for water tank experiments with varying water depths and different bottom characteristics. An analysis of the experiment suggests that diffused light and its specular reflection contribute significantly to reflectance and cannot be ignored. This observation is significant, as these parameters are often ignored. The study also illustrates that tank experiments are an important first step in testing and validating various models of reflectance before they can be utilized in field experiments to assess water quality.

Acknowledgements

This study was funded by U.S. Environmental Protection Agency (Grant No. X7-97654601-0) and by the University of Arkansas - Division of Agriculture. We thank Dr. Sreekala G. Bajwa for providing the spectroradiometer for experimental data collection. Comments by Dr. K. P. Sudheer, two anonymous reviewers, and Dr. Barry Allred helped improve the earlier versions of the manuscript.

REFERENCES

Aas, E. 1987. Two-stream irradiance model for deep waters. *Appl. Optics* 26(11): 2095-2101.

Allee, R. J., and J. E. Johnson. 1999. Use of satellite imagery to estimate surface chlorophyll *a* and Secchi disc depth of Bull Shoals reservoir, Arkansas, USA. *Intl. J. Remote Sensing* 20(6): 1057-1072.

Arst, H. 2003. *Optical Properties and Remote Sensing of Multicomponental Water Bodies*. Chichester, U.K.: Praxis Publishing.

Baruah, P. J. 2000. Application of remote sensing and smart algorithms for modeling of water quality in Lake Kasumigaura. PhD diss. Tsukuba, Japan: University of Tsukuba.

Bhargava, D. S., and D. W. Mariam. 1990. Spectral reflectance relationships to turbidity generated by different clay materials. *Photogram. Eng. and Remote Sensing* 56(2): 225-229.

Bhargava, D. S., and D. W. Mariam. 1991a. Effects of suspended particle size and concentration on reflectance measurements. *Photogram. Eng. and Remote Sensing* 57(5): 519-529.

Bhargava, D. S., and D. W. Mariam. 1991b. Light penetration depth, turbidity, and reflectance related relationships and models. *ISPRS J. Photogram. and Remote Sensing* 46(4): 217.

Brivio, P. A., C. Giardino, and E. Zilioli. 2001. Determination of chlorophyll concentration changes in Lake Garda using an image-based radiative transfer code for Landsat TM images. *Intl. J. Remote Sensing* 22(2-3): 487-502.

Chipman, J. W., T. M. Lillesand, J. E. Schmaltz, J. E. Leale, and M. J. Nordheim. 2004. Mapping lake water clarity with Landsat images in Wisconsin, USA. *Canadian J. Remote Sensing* 30(1): 1-7.

Choubey, V. K. 1994. Monitoring water quality in reservoirs with IRS-1A-LISS-I. *Water Resour. Mgmt.* 8(2): 121-136.

Doxaran, D., R. C. Nagur Cherukuru, and S. J. Lavender. 2004. Estimation of surface reflection effects on upwelling radiance field measurements in turbid waters. *J. Optics A: Pure and Applied Optics* 6(7): 690-697.

Doyle, J. P., and H. Rief. 1998. Photon transport in three-dimensional structures treated by random walk techniques: Monte Carlo benchmark of ocean colour simulations. *Math. Comput. Simul.* 47(2-5): 215-241.

Fraser, R. N. 1998. Multispectral remote sensing of turbidity among Nebraska Sand Hills lakes. *Intl. J. Remote Sensing* 19(15): 3011-3016.

Garg, V. 2006. Development and evaluation of a physical hyperspectral optical-Monte Carlo model for an aquatic medium reflectance simulation. PhD diss. Fayetteville, Ark.: University of Arkansas.

Garg, V., I. Chaubey, C. Maringanti, and S. G. Bajwa. 2009. Modeling spectral reflectance of Beaver Reservoir using pseudo neural network simulator of a remote sensing model and genetic algorithm optimizer. *Trans. ASABE* (in review).

Gordon, H. R., O. B. Brown, and M. M. Jacobs. 1975. Computed relationships between the inherent and apparent optical properties of a flat homogeneous ocean. *Appl. Optics* 14(2): 417-427.

Han, L. 1997. Spectral reflectance with varying suspended sediment concentrations in clear and algae-laden waters. *Photogram. Eng. and Remote Sensing* 63(6): 701-705.

Han, L. H., and D. C. Rundquist. 1996. Spectral characterization of suspended sediments generated from two texture classes of clay soil. *Intl. J. Remote Sensing* 17(3): 643-649.

Han, L., and D. C. Rundquist. 2003. The spectral responses of *Ceratophyllum demersum* at varying depths in an experimental tank. *Intl. J. Remote Sensing* 24(4): 859-864.

Harrington, J. A., F. R. Schiebe, and J. F. Nix. 1992. Remote sensing of Lake Chicot, Arkansas: Monitoring suspended sediments, turbidity, and Secchi depth with Landsat MSS data. *Remote Sensing Environ.* 39(1): 15-27.

IOCCG. 2000. Report 3: Remote sensing of ocean colour in coastal and other optically complex waters. S. Sathyendranath, ed. Dartmouth, Nova Scotia, Canada: International Ocean-Colour Coordinating Group. Available at: www.ioccg.org/reports_ioccg.html. Accessed 5 May 2005.

Kirk, J. T. O. 1984. Dependence of relationship between inherent and apparent optical properties of water on solar altitude. *Limnol. Oceanogr.* 29(2): 350-356.

Kloiber, S. N., P. L. Brezonik, L. G. Olmanson, and M. E. Bauer. 2002. A procedure for regional lake water clarity assessment using Landsat multispectral data. *Remote Sensing Environ.* 82(1): 38-47.

Lathrop, R. G., T. M. Lillesand, and B. S. Yandell. 1991. Testing the utility of simple multi-date thematic mapper calibration algorithms for monitoring turbid inland waters. *Intl. J. Remote Sensing* 12(10): 2045-2063.

Lodhi, M. A., and D. C. Rundquist. 2001. A spectral analysis of bottom-induced variation in the colour of Sand Hills lakes, Nebraska, USA. *Intl. J. Remote Sensing* 22(9): 1665-1682.

Lodhi, M. A., D. C. Rundquist, L. H. Han, and M. S. Kuzila. 1997. The potential for remote sensing of loess soils suspended in surface waters. *JAWRA* 33(1): 111-117.

Mantovani, J. E., and A. P. Cabral. 1992. Tank depth determination for water radiometric measurements. *Intl. J. Remote Sensing* 13(14): 2727-2733.

Marcus, W. A., and M. A. Fonstad. 2007. Optical remote mapping of rivers at sub-meter resolution and watershed extents. *Earth Surface Proc. and Landforms* 33(1): 4-24.

Mobley, C. D. 1994. *Light and Water: Radiative Transfer in Natural Waters.* San Diego, Cal.: Academic Press.

Mobley, C. D., and L. K. Sundman. 2003. Effects of optically shallow bottoms on upwelling radiances: Inhomogeneous and sloping bottoms. *Limnol. Oceanogr.* 48(1, part 2): 329-336.

Mobley, C. D., B. Gentili, H. R. Gordon, Z. H. Jin, G. W. Kattawar, A. Morel, P. Reinersman, K. Stamnes and R. H. Stavn. 1993. Comparison of numerical models for computing underwater light fields. *Appl. Optics* 32(36): 7484-7504.

Mobley, C. D., H. Zhang, and K. J. Voss. 2003. Effects of optically shallow bottoms on upwelling radiances: Bidirectional reflectance distribution function effects. *Limnol. Oceanogr.* 48(1, part 2): 337-345.

Mobley, C. D., W. P. Bissett, J. H. Bowles, C. O. Davis, T. V. Downes, A. Gleason, D. D. R. Kohler, R. A. Leathers, E. M. Lochard, M. J. Montes, R. P. Reid, and L. K. Sundman. 2005. Interpretation of hyperspectral remote-sensing imagery via spectrum matching and look-up tables. *Appl. Optics* 44(17): 3576-3592.

Morel, A., and B. Gentili. 1993. Diffuse reflectance of oceanic waters: II. Bidirectional aspects. *Appl. Optics* 32(33): 6864-6879.

Morel, A., and B. Gentili. 1996. Diffuse reflectance of oceanic waters: III. Implication of bidirectionality for the remote sensing problem. *Appl. Optics* 35(24): 4850-4862.

Morel, A., and S. Maritorena. 2001. Bio-optical properties of oceanic waters: A reappraisal. *J. Geophys. Res.* 106(C4): 7163-7180.

Morel, A., and L. Prieur. 1977. Analysis of variations in ocean color. *Limnol. Oceanogr.* 22(4): 709-722.

Nanu, L., and C. Robertson. 2004. The effect of suspended sediment depth distribution on coastal water spectral reflectance: Theoretical simulation. *Intl. J. Remote Sensing* 14(2): 225-239.

Panda, S. S., V. Garg, and I. Chaubey. 2004. Artificial neural network applications in lake water quality estimation using satellite imagery. *J. Environ. Informatics* 4(2): 65-74.

Pope, R. M., and E. S. Fry. 1997. Absorption spectrum (380-700 nm) of pure water: II. Integrating cavity measurements. *Appl. Optics* 36(33): 8710-8723.

Prahl, S. A., M. Keijzer, S. L. Jacques, and A. J. Welch. 1989. A Monte Carlo model of light propagation in tissue. In *SPIE*

Proceedings of Dosimetry of Laser Radiation in Medicine and Biology, 102-111. Bellingham, Wash.: SPIE.

Ritchie, J. C., and C. M. Cooper. 1991. An algorithm for estimating surface suspended sediment concentrations with Landsat MSS digital data. *Water Resour. Bull.* 27(3): 373-379.

Ritchie, J. C., C. M. Cooper, and F. R. Schiebe. 1990. The relationship of MSS and TM digital data with suspended sediments, chlorophyll, and temperature in Moon Lake, Mississippi. *Remote Sensing Environ.* 33(2): 137-148.

Ritchie, J. C., F. R. Schiebe, C. M. Cooper, and J. A. Harrington. 1994. Chlorophyll measurements in the presence of suspended sediment using broadband spectral sensors aboard satellites. *J. Freshwater Ecol.* 9(3): 197-205.

Ritchie, J. C., P. V. Zimba, and J. H. Everitt, 2003. Remote sensing techniques to assess water quality. *Photogram. Eng. and Remote Sensing* 69(6): 695-704.

Schiebe, F. R., J. A. Harrington, and J. C. Ritchie. 1992. Remote sensing of suspended sediments: The Lake Chicot, Arkansas project. *Intl. J. Remote Sensing* 13(8): 1487-1509.

Singh, N., S. G. Bajwa, and I. Chaubey. 2008. Removal of surface reflectance from above-water visible-near infrared spectroscopic measurements. *Applied Spectroscopy* 62(9): 1013-1021.

Smith, R. C., and K. S. Baker. 1981. Optical properties of the clearest natural waters (200-800 nm). *Appl. Optics* 20(2): 177-184.

Stamnes, K., W. Li, B. Yan, H. Eide, A. Barnard, W. S. Pegau, and J. J. Stamnes. 2003. Accurate and self-consistent ocean color algorithm: Simultaneous retrieval of aerosol optical properties and chlorophyll concentrations. *Appl. Optics* 42(6): 939-951.

Stramski, D., E. Boss, D. Bogucki, and K. J. Voss. 2004. The role of seawater constituents in light backscattering in the ocean. *Prog. Oceanogr.* 61(1): 27-56.

Sudheer, K. P., I. Chaubey, and V. Garg. 2006. Lake water quality assessment from Landsat TM data using neural network: An approach to optimal band combination selection. *JAWRA* 42(6): 1683-1695.

Tolk, B. L., L. Han, and D. C. Rundquist. 2000. The impact of bottom brightness on spectral reflectance of suspended sediments. *Intl. J. Remote Sensing* 21(11): 2259-2268.

Yacobi, Y. Z., A. Gitelson, and M. Mayo. 1995. Remote sensing of chlorophyll in Lake Kinneret using high-spectral-resolution radiometer and Landsat TM: Spectral features of reflectance and algorithm development. *J. Plankton Res.* 17(11): 2155-2173.

Yang, M., C. J. Merry, and R. M. Sykes. 1999. Integration of water quality modeling, remote sensing, and GIS. *JAWRA* 35(2): 253-263.